

# *Experimental Characterization and Correlation of a Triangular Channel Geometry PEM Fuel Cell at Different Operating Conditions*

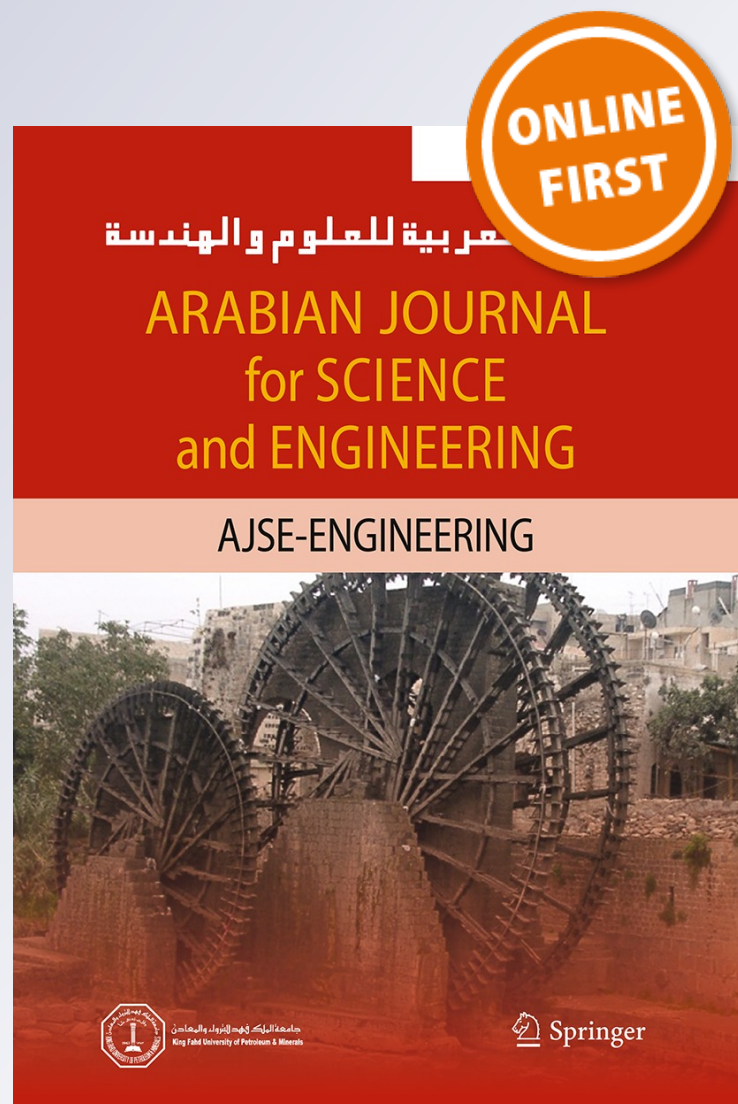
**I. Khazae & M. Ghazikhani**

**Arabian Journal for Science and Engineering**

ISSN 1319-8025

Arab J Sci Eng

DOI 10.1007/s13369-013-0605-2



**Your article is protected by copyright and all rights are held exclusively by King Fahd University of Petroleum and Minerals. This e-offprint is for personal use only and shall not be self-archived in electronic repositories. If you wish to self-archive your work, please use the accepted author's version for posting to your own website or your institution's repository. You may further deposit the accepted author's version on a funder's repository at a funder's request, provided it is not made publicly available until 12 months after publication.**

# Experimental Characterization and Correlation of a Triangular Channel Geometry PEM Fuel Cell at Different Operating Conditions

I. Khazaei · M. Ghazikhani

Received: 2 September 2011 / Accepted: 2 December 2011  
© King Fahd University of Petroleum and Minerals 2013

**Abstract** In this study, the performance of a 10 W PEM fuel cell with 25 cm<sup>2</sup> active area and Nafion 117 as membrane with 0.004 g/cm<sup>2</sup> platinum for the anode and cathode and triangular channel geometry is investigated experimentally. The effect of some important parameters such as input oxygen and hydrogen temperatures ( $T_{O_2}$ ,  $T_{H_2}$ ), cell temperature ( $T_{cell}$ ), input pressure ( $P$ ), and oxygen ( $\dot{Q}_{O_2}$ ) and hydrogen flow rates ( $\dot{Q}_{H_2}$ ) investigated on the performance of the cell. An experimental equation is offered with least square method to correlate the data for the polarization curve. The results show that with increasing the input temperature of the oxygen and hydrogen from 45 to 65 °C and 40 to 60 °C, the performance of the cell increases about 20 %. Also the results show that with increasing the cell temperature from 45 to 65 °C, the performance of the cell increases about 18 %.

**Keywords** Fuel cell · Curve fitting · Performance · Operating parameters

I. Khazaei (✉)  
Department of Mechanical Engineering, Torbat-e-jam branch,  
Islamic Azad University,  
Torbat-e-jam, Iran  
e-mail: imankhazaei@yahoo.com

I. Khazaei · M. Ghazikhani  
Engineering Faculty, Mechanical Engineering Department,  
Ferdowsi University of Mashhad, P. O. Box 9177948944-1111,  
Mashhad, Iran

I. Khazaei · M. Ghazikhani  
Department of Mechanical and Energy Engineering,  
Power and Water University of Technology,  
16765-1719 Tehran, Iran

## الخلاصة

تم - في هذه الدراسة - التحقيق تجريبيا في أداء خلية الوقود PEM W10 مع منطقة نشطة بمساحة 25 سم<sup>2</sup> و Nafion 117 كغشاء مع 0.004 غم/سم<sup>2</sup> بلاتين للأنود والكاثود وهندسة القناة المثلثة. وتم البحث في تأثير بعض المعاملات الهامة مثل درجات حرارة الأوكسجين والهيدروجين المدخلين ( $T_{O_2}$ ) و ( $T_{H_2}$ )، ودرجة حرارة الخلية ( $T_{cell}$ )، وضغط الإدخال ( $P$ )، ومعدلات تدفق الأوكسجين والهيدروجين ( $\dot{Q}_{O_2}$  و ( $\dot{Q}_{H_2}$ ) في أداء الخلية. وقدمت معادلة تجريبية مع طريقة التربيع الأقل لربط البيانات لأجل منحنى الاستقطاب. وبينت النتائج أنه مع زيادة درجة حرارة الأوكسجين والهيدروجين المدخلين من 45 م° إلى 65 م° ومن 40 م° إلى 60 م° فإن أداء الخلية يزداد حوالي 20%. كما أظهرت النتائج أنه مع زيادة درجة حرارة الخلية من 45 م° إلى 65 م° فإن أداء الخلية يزداد حوالي 18%.

## List of Symbols

$a$	Constant parameter
$I$	Current (A)
$n$	Variable number
$\dot{Q}_{H_2}$	Hydrogen flow rate (L/min)
$\dot{Q}_{O_2}$	Oxygen flow rate (L/min)
$T_{cell}$	Cell temperature (°C)
$T_{H_2}$	Input hydrogen temperature (°C)
$T_{O_2}$	Input oxygen temperature (°C)
$V$	Cell potential (V)
$Y_i$	Input data
$Z$	Shape parameter of channels

## Greek Symbols

$\sigma_i$	Measurement error
$\hat{\beta}_j$	Regression parameter
$\chi$	Merit function

## 1 Introduction

A fuel cell is an electro-chemical energy device that converts the chemical energy of fuel directly into electricity and

heat, with water as a by-product of the reaction. Based on the types of electrolytes used, they are categorized into polymer electrolyte membrane fuel cell (PEMFC), solid oxide fuel cells (SOFCs), phosphoric acid fuel cells (PAFCs), molten carbonate fuel cells (MCFCs), and direct methanol fuel cells (DMFCs). The proton exchange membrane fuel cell (PEMFC) is considered to be the most promising candidate for electric vehicles by virtue of its high power density, zero pollution, low operating temperature, quick start-up capability, and long lifetime.

Furthermore, the PEM fuel cell is being investigated as an alternate power generation system especially for distributed generation and transportation. The PEM fuel cell is providing reliable power at steady state; however, it is not able to respond promptly to a load step change. Since the fuel cell is an electrochemical energy conversion device that converts fuel into electricity, its dynamic behavior depends both on chemical and thermodynamic processes [1]. The polymer electrolytes work at low temperature, which brings this further advantage that a PEM fuel cell can start quickly. PEM fuel cells are being actively developed for use in cars and buses, as well as for a very wide range of portable applications, and also for combined heat and power systems. It could be argued that PEM fuel cells exceed all other electrical energy generating technologies in the breadth of scope of their possible applications.

Scrivano et al. [2] presented the results of an experimental analysis performed on an Exchange miniaturized, 6 W Proton Membrane Fuel Cell (PEMFC) system, integrated with on-site hydrogen production by electrolysis; in particular, they investigated the effects of environmental parameters such as the external temperature and the humidity on the performance of fuel cells. Also, they proposed a simple semi-empirical mathematical model capable to perform rough prediction on the behavior of such systems when exposed at different ambient temperatures. The model treats the stacks as black boxes, not investigating singularly the inner phenomena which occur in the cell.

Amphlett et al. [3,4] investigated a theoretical model which was employed to provide the structure of the equations, and then, the parameters of these equations were found using the regression techniques to fit the experimental results. Also, they studied a semi-empirical model with a theoretical background that takes into account the main variables of the fuel cell operation such as the operating temperature, the partial pressures at the electrodes and the fuel cell current.

Del Real et al. [5] investigated a simple empirical equation to model the fuel cell voltage with considering the variations of the main process variables. The model equation has 11 parameters: one parameter related to the mass of liquid water at the anode channel must be estimated due to technical constraints, and the other parameters are obtained from experimental data. Although the model proposed by them,

fitted well with the experimental data, the equation of the fuel cell voltage does not have a theoretical basis, and, therefore, it is based on assumptions relating to the effects of temperature and partial pressures that are not proven to be general for fuel cells other than those used in [5].

Berning and Djilali [6] using a three-dimensional computational model for a single cell with an active area of 25 cm<sup>2</sup> and single-serpentine flow field, investigated the influence of this parameter on the cell performance.

Yi and Nguyen [7] used the numerical methods to solve a two-dimensional single-phase polymer electrolyte membrane fuel cell model with interdigitated flow channels so as to evaluate the effects of inlet and exit pressures, gas diffusion layer thickness and carbon plate width on the performance of polymer electrolyte membrane fuel cell.

Xue and Dong [8] used a semi-empirical model of the Ballard Mark IV fuel cell and models for the auxiliary systems to create a model of the fuel cell system. Using this model and numerical optimization, the optimal active stack area and air stoichiometric ratio were obtained to maximize net power output, and at the same time, minimized production costs.

Ferng et al. [9] performed analytical and experimental work to investigate a single PEM fuel cell. In their paper, they presented a study of the cell performance covering the effects of operating temperature and pressure on performance and the flow characteristics within the cell. Their paper shows the positive effects of temperature and pressure on the performance of a single PEM fuel cell.

Hussain et al. [10] investigated a thermodynamic model of a PEM fuel cell power system for transportation applications. Their analysis includes the operation of all the components in the system, which consists of two major modules: PEM fuel cell stack module and system module and a cooling pump. System module includes air compressor, heat exchanger, humidifier and a cooling loop. They found that with the increase of external load (current density), the difference between the gross stack power and net system power increases and the largest irreversibility rate occurs in the fuel cell stack.

Park and Xianguo [11] investigated a numerical and experimental study to investigate the cross flow in a PEM fuel cell. Experimental measurements revealed that the pressure drop in a PEM fuel cell is significantly lower than that without cross flow, and three-dimensional numerical simulation has been performed for wide ranges of flow rate, permeability and thickness of gas diffusion layer to analyze the effects of those parameters on the resultant cross flow and the pressure drop of the reactant streams.

Jiao et al. [12] investigated the characteristics of liquid water removal from GDL experimentally, through measuring unsteady pressure drop in a cell which has the GDL initially wet with liquid water. They controlled the thickness of GDL carefully by inserting various thicknesses of



metal shims between the plates. They found that severe compression of GDL could result in excessive pressure drop from channel inlet to channel outlet.

Park and Xianguo [13] developed a non-isothermal stack model to analyze the effects of flow variance and temperature distribution on the performance of a PEM fuel cell stack. Their stack model consists of the flow network solver for pressure and mass flow distributions for the reactant gas streams and cooling water, and the heat transfer solver for temperature distribution among the cells in the stack, as well as the fuel cell model for individual cell performance. They found that the effect of temperature is dominant on the cell voltage variance when the flow variance is small for sufficiently uniform distribution of reactant flow among the cells in the stack.

In the present work, the effects of oxygen and hydrogen temperature, cell temperature, input pressure, and oxygen and hydrogen flow rate on the performance of a PEM fuel cell with triangular channel have been studied experimentally. Several polarization curves have been obtained in different conditions, displaying the trend of the cell voltage against current. The objective of this paper is to analyze the influence of all discussed parameters on the performance of the PEM fuel cell at different levels of cell current. Also for obtained results, a semi empirical equation for polarization curve with the change in the input gases temperature, pressure and flow rate and cell temperature for PEM fuel cell developed that can be used in different values of above parameters.

## 2 Description of the Experiments

For experimental investigation of the performance of the fuel cell, a setup has been fabricated. A schematic flow of the test bench is shown in Fig. 1. It allows controlling several physical parameters, and the measurement of many output data. In fact, the polymeric membrane has permeability to hydrogen

and oxygen; due to the high-pressure gradient from cathode to anode, this driving force could push hydrogen from cathode to anode across the membrane and a dangerous mix with oxygen could occur; this concentration must always be kept below a safety level.

The test bench is made up of four main subsystems. First, the gases supply system, which sends the oxygen and hydrogen flow into the system for electrochemical reaction. Second, there is two humidifiers that humidify the oxygen and hydrogen before going into the cell for complete transferring of proton from the membrane to the cathode side. Third, the nitrogen supply system is applied to inert any flammable mix inside the ducts and to purge the system before activation. Finally, there is the electrical power supply, regulated from an AC/DC voltage regulator driven from the control panel.

The specifications of the test system for this study are:

- The humidifier system is membranous.
- The test bench has the system of announcement the leakage of hydrogen.
- The system can control and show the temperature of the oxygen and hydrogen.
- The system can control and show the temperature of the cell.
- The system can control and show the flow rate of the oxygen and hydrogen.
- The system can control and show the inlet pressure of the oxygen and hydrogen.
- The system can show the voltage of the cell.
- The system can show the current of the cell.

Table 1 shows the environs of operation of the experimental setup in this study.

The PEM fuel cell considered in this study is a single cell with the size of  $45 \times 95 \times 101 \text{ mm}^2$  and an active area of  $25 \text{ cm}^2$ , and serpentine and triangular flow field

**Fig. 1** Schematic of the polymer electrolyte membrane fuel cell system

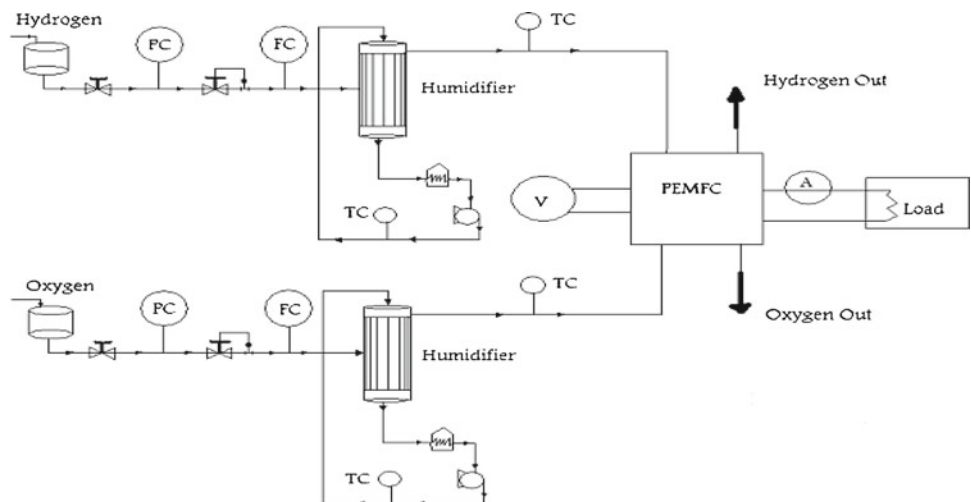


**Table 1** Operational characteristics of the test bench

Voltage (V)	0–2
Current (A)	0–20
Power (W)	0–22
Moisture (%)	100
Flow rate (L/min)	0–2
Gases temperature (°C)	Up to 75
Cell temperature (°C)	Up to 75

geometries of channels with the weight of 1,300 g. The width, land width, and depth of the channel were selected to be 1, 0.8, and 2 mm, respectively. For a bipolar plate, non-porous graphite is selected. A Nafion 117 membrane with 0.004 g/cm<sup>2</sup> platinum for the anode and cathode was employed as a membrane electrode assembly. On both sides of the MEA, there were 0.33 mm thick carbon papers that acted as diffusion layers. The thickness of the catalyst layer and the proton exchange membrane is about 0.01 and 0.051 mm. The geometry of the channels of the cell in the experimental setup is shown in Fig. 2.

### 3 Method of the Measurements

The examined prototype can operate at a maximum 5 bar absolute pressure; a pressure regulator valve is included, to make possible to vary the operating pressure of the FC system, and the accuracy of monitoring the pressure is ±2 %. Two flow meters is used to measure the flow rate of the oxygen and hydrogen that the accuracy of them is ±0.1 L/min.

In order to plot the polarization curve and simulate a variable load, a resistors box was used that the accuracy of monitoring the voltage and ampere is ±1 %. The resistors box, located outside the test chamber, is manually operated; the box and the cables do not introduce relevant errors because

they are shielded from external magnetic fields (due to the very low current values). In order to operate in equilibrium conditions, current and voltage values corresponding to each particular value of the total resistance were measured after a sufficient time period to ensure stationary conditions to have been reached as concerns both fuel cell performance and the values of humidity and temperature in the test chamber. The temperature of the inlet gases was measured by digital thermometer with ±0.1 °C accuracy.

The changed parameters are: input oxygen temperature ( $T_{O_2}$ ), input hydrogen temperature ( $T_{H_2}$ ), cell temperature ( $T_{cell}$ ), input pressure ( $P$ ), oxygen ( $\dot{Q}_{O_2}$ ) and hydrogen flow rates ( $\dot{Q}_{H_2}$ ) and the measured parameters are voltage and current of the cell.

At first, we perform the experiments by humidifying the membrane of the fuel cell by saturation water vapor and then change the input oxygen and hydrogen temperatures, cell temperature, input pressure, oxygen and hydrogen flow rates and measure the pointed parameters and the voltage and the current of the cell after steady state condition. Figure 3 shows the experimental setup.

### 4 Results and Discussion

The range of changing the parameters in this study is shown in Table 2 and the experiments for each of the parameters done and repeated while the steady state condition occurred.

In Figs.4 and 5, the effect of hydrogen and oxygen flow rates of the anode and cathode sides at the overall cell performance of the triangular channel geometry PEM fuel cell for  $T_{cell} = 60\text{ }^\circ\text{C}$ ,  $T_{O_2} = 55\text{ }^\circ\text{C}$ ,  $T_{H_2} = 55\text{ }^\circ\text{C}$ ,  $\dot{Q}_{O_2} = 0.5\text{ L/min}$  and  $P = 2.905\text{ bar}$  are shown. It is clear that by increasing the hydrogen flow rate from 0.3 to 0.7 L/min and the oxygen flow rate from 0.5 to 0.9 L/min, the cell performance enhances but when the flow rate increases from 0.7 to 0.9 L/min for hydrogen and from 0.9 to 1.3 L/min, the cell

**Fig. 2** Schematic of the channels polymer electrolyte membrane fuel cell

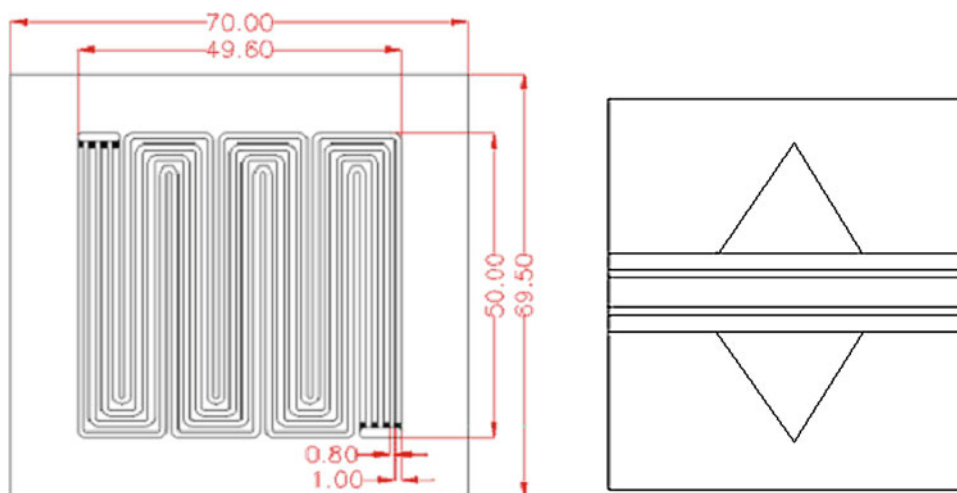


**Fig. 3** Schematic of the experimental setup

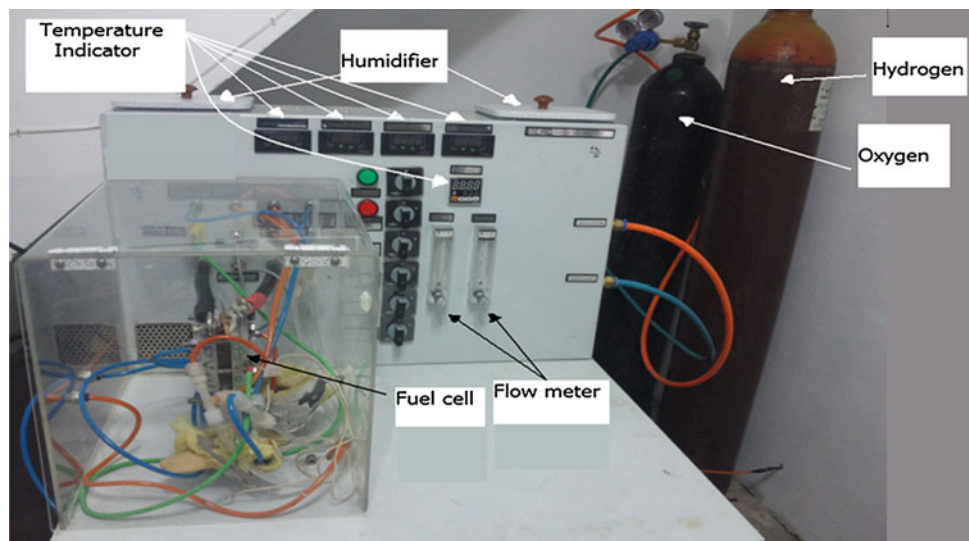


**Table 2** Range of changing the parameters in this study

Description	Value
Oxygen flow rate (L/min)	0.5–1.3
Hydrogen flow rate (L/min)	0.3–1.3
Anode inlet pressure (bar)	1–4
Cathode inlet pressure (bar)	1–4
Cell temperature (°C)	40–60
Oxygen temperature (°C)	45–65
Hydrogen temperature (°C)	40–60

performance decreases. It is due to that by increasing the flow rate of hydrogen and oxygen, more fuel and oxidizer transport from GDL to the catalyst layer and the electrochemical reaction enhances; but when the flow rate of hydrogen and oxygen increases from 0.7 to 0.9 L/min, the transportation of fuel and oxidizer to the GDL decrease and they come out from the channel without an electrochemical reaction.

Figure 6 shows the effect of cell temperature on the performance of the cell at  $P = 2.905$  bar,  $T_{O_2} = 55$  °C,  $T_{H_2} = 55$  °C,  $\dot{Q}_{O_2} = 0.5$  L/min and  $\dot{Q}_{H_2} = 0.3$  L/min. It is clear that increasing cell temperature leads to the increase in the performance of the cell which is due to the decreasing of activation overpotential and increase in the electrochemical reaction. This is because of the exchange current density of the oxygen reduction reaction increases rapidly with temperature due to the enhanced reaction kinetics, which reduces activation losses. A higher temperature leads also to a higher diffusivity of the hydrogen protons in the electrolyte membrane, thereby reducing the membrane resistance and this leads to reducing the potential loss in the membrane. Also, Fig. 6 indicates that at the conditions of the higher operating voltage (lower overpotential), the influence of the internal flow modification on the overall fuel cell performance is

negligibly small. At lower operating voltage conditions, on the other hand, the effect of the internal flow modification on the polarization curves becomes important.

The temperature basically affects all the different transport phenomena inside the fuel cell. The composition of the incoming gas streams depends strongly on the temperature. Assuming the inlet gases are fully humidified, the partial pressure of water vapor entering the cell depends on the temperature only. Thus, the molar fraction of water vapor is a function of the total inlet pressure and temperature, and so the molar fraction of the incoming hydrogen and oxygen depends on the temperature and pressure as well. In Figs. 7 and 8, the effects of input hydrogen and oxygen temperatures of the anode and cathode sides at the overall cell performance of the triangular channel geometry PEM fuel cell for  $T_{cell} = 60$  °C,  $\dot{Q}_{H_2} = 0.3$  L/min,  $\dot{Q}_{O_2} = 0.5$  L/min and  $P = 2.905$  bar are shown. It is clear that at the conditions of the higher operating voltage (lower overpotential), the influence of the oxygen temperature on the overall fuel cell performance is negligibly small but at lower operating voltage conditions, the effect of input temperature on the polarization curves becomes important. Also, it is clear that by increasing the hydrogen and oxygen temperatures, the cell performance enhances that it is due to the decreasing of activation overpotential and increase in the electrochemical reaction at the catalyst surfaces.

#### 4.1 Developing a New Correlation for Polarization Curve

By doing the experiments, it is clear that some parameters such as input oxygen ( $T_{O_2}$ ) and hydrogen temperatures ( $T_{H_2}$ ), cell temperature ( $T_{cell}$ ), input pressure ( $P$ ), oxygen ( $\dot{Q}_{O_2}$ ) and hydrogen flow rates ( $\dot{Q}_{H_2}$ ) affect the performance of the cell. The main reason of changing the performance by changing these parameters is the electrochemical reaction at the

**Fig. 4** Variation of cell performance at different hydrogen flow rates for  $T_{cell} = 60^{\circ}C$ ,  $\dot{Q}_{O_2} = 0.5\text{ L/min}$ ,  $P = 2.905\text{ bar}$ ,  $T_{O_2} = 55^{\circ}C$  and  $T_{H_2} = 55^{\circ}C$

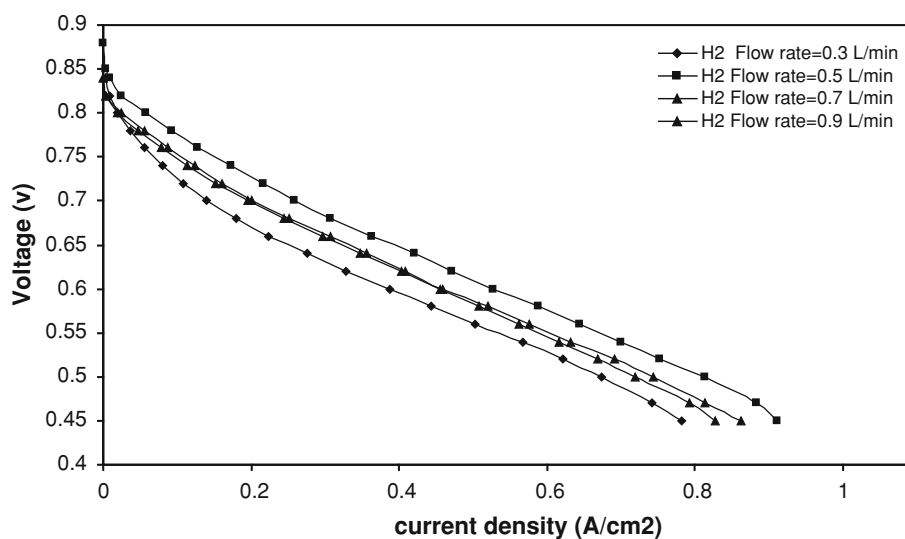


**Fig. 5** Variation of cell performance at different oxygen flow rates for  $T_{cell} = 60^{\circ}C$ ,  $\dot{Q}_{H_2} = 0.3\text{ L/min}$ ,  $P = 2.905\text{ bar}$ ,  $T_{O_2} = 55^{\circ}C$  and  $T_{H_2} = 55^{\circ}C$

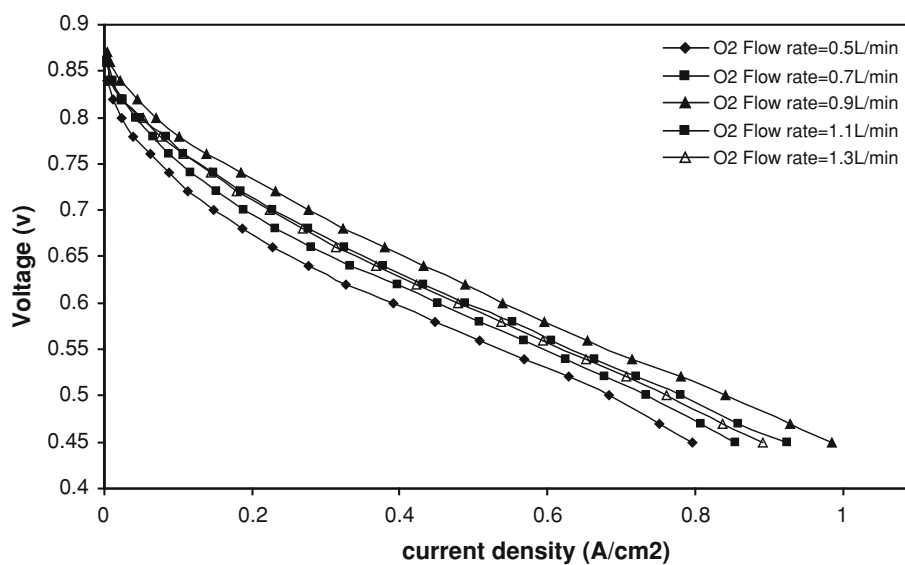


**Fig. 6** Variation of cell performance at different cell temperatures for  $P = 2.905\text{ bar}$ ,  $\dot{Q}_{H_2} = 0.3\text{ L/min}$ ,  $\dot{Q}_{O_2} = 0.5\text{ L/min}$ ,  $T_{O_2} = 55^{\circ}C$  and  $T_{H_2} = 55^{\circ}C$

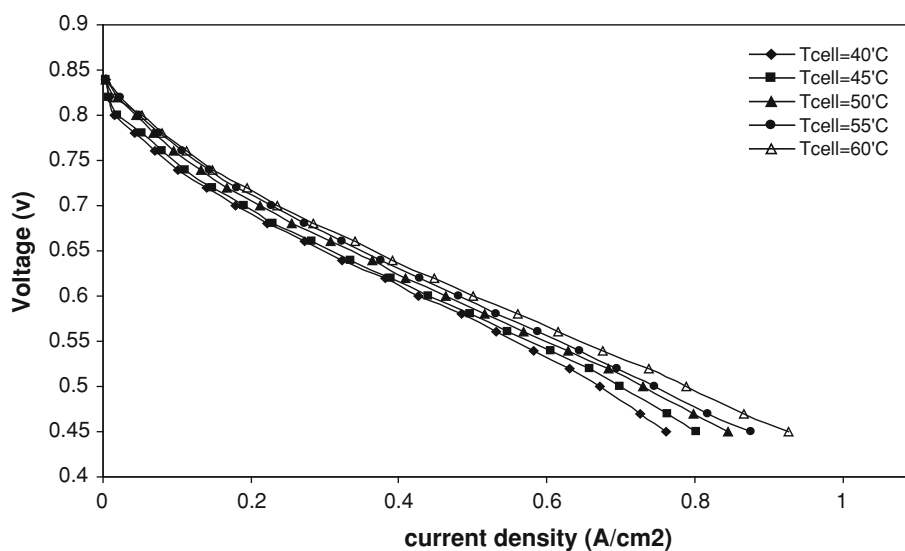




**Fig. 7** Variation of cell performance at different hydrogen temperatures for  $P = 2.905$  bar,  $\dot{Q}_{H_2} = 0.3$  L/min,  $\dot{Q}_{O_2} = 0.5$  L/min,  $T_{O_2} = 55^\circ\text{C}$  and  $T_{\text{cell}} = 60^\circ\text{C}$

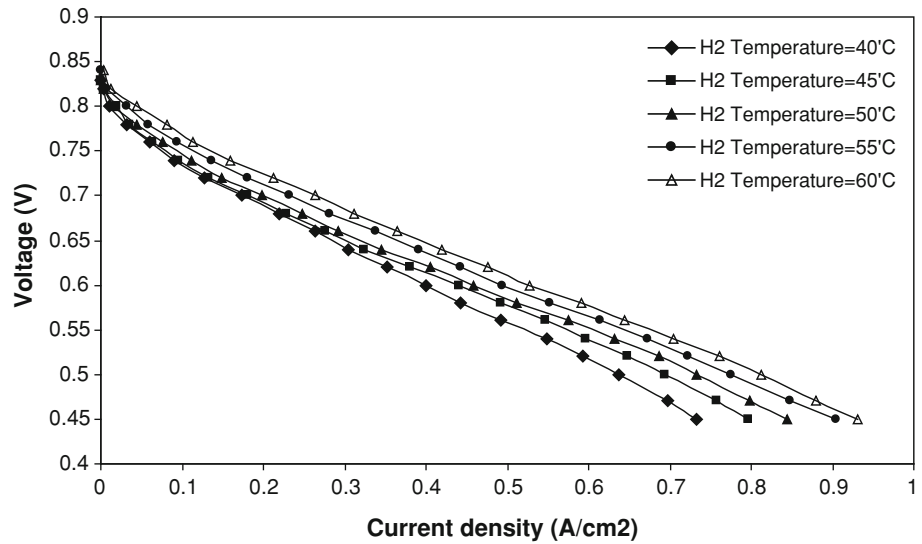
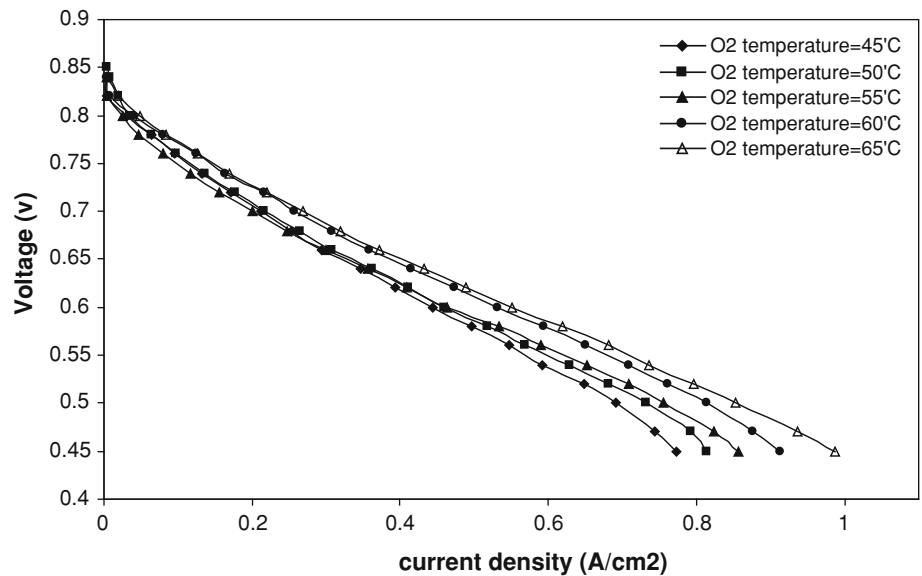


**Fig. 8** Variation of cell performance at different oxygen temperatures for  $P = 2.905$  bar,  $\dot{Q}_{H_2} = 0.3$  L/min,  $\dot{Q}_{O_2} = 0.5$  L/min,  $T_{H_2} = 55^\circ\text{C}$  and  $T_{\text{cell}} = 60^\circ\text{C}$



catalyst surfaces but the more details described in previous sections. The method of fitting used in this paper is the least square method. This method fits a set of data points  $(x_i, y_i)$  to a function that is a combination of any number of functions of the independent variable  $x$ . The goal of nonlinear regression is to determine the best-fit parameters for a model by minimizing a chosen merit function. Where nonlinear regression differs is that the model has a nonlinear dependence on the unknown parameters, and the process of merit function minimization is an iterative approach. The process is to start with some initial estimates and incorporates algorithms to improve the estimates iteratively. The new estimates then become a starting point for the next iteration. These iterations continue until the merit function effectively stops decreasing. The nonlinear model to be fitted can be represented by:

$$y = y(x; a) \tag{1}$$

The merit function minimized in performing nonlinear regression the following:

$$\chi^2(a) = \sum_{i=1}^N \left\{ \frac{y_i - y(x_i; a)}{\sigma_i} \right\}^2 \tag{2}$$

where  $\sigma_i$  is the measurement error, or standard deviation of the  $i$ th data point. For understanding how the results calculated we have:

The  $i$ th predicted, or fitted value of the dependent variable  $Y$ , is denoted by  $\hat{Y}_i$ . This value is obtained by evaluating the regression model  $\hat{Y} = f(X, \hat{\beta}_j)$ , where  $\hat{\beta}_j$  is the regression parameter, or variable. Then, the residuals  $(Y_i - \hat{Y}_i)$  and sum

**Table 3** Value and limits of constants in Eq. (3)

Variable	Value	Lower limit	Upper limit
<i>a</i>	0.872654001	0.868892869	0.876415133
<i>b</i>	-0.191011137	-0.199909826	-0.182112449
<i>c</i>	-0.27134189	-0.284603833	-0.258079947
<i>d</i>	-9.97E-02	-0.13058875	-6.87E-02
<i>e</i>	-0.1375914	-0.173141973	-0.101980826
<i>f</i>	-2.69E-02	-3.41E-02	-1.97E-02
<i>g</i>	-0.132698922	-0.153154262	-0.112243582
<i>h</i>	13.85642525	-3.472674784	31.18552528
<i>m</i>	-6.228078322	-124,161.6701	31.18552528
<i>j</i>	1.775427703	-59,501.80159	59,505.35244
<i>k</i>	0.368901517	0.33917133	0.398631704
<i>l</i>	7.89E-04	-137.8906155	137.8921933
<i>n</i>	0.216711724	0.195475458	0.23794799
<i>p</i>	0.548819575	-18,393.17559	18,394.27323

of the residuals  $\sum_{i=1}^n (Y_i - \hat{Y}_i)$  calculated and then, the average of residuals and residual of sum of squares calculated.

$$SSE = \text{Residual or Error Sum of Squares (Absolute)} = \sum_{i=1}^n (Y_i - \hat{Y}_i)^2$$

$$SSE_R = \text{Residual or Error Sum of Squares (Relative)} = \sum_{i=1}^n [(Y_i - \hat{Y}_i)^2 * W_i]$$

where  $W_i = 1/\sigma_i^2$  normalized so that  $\sum_{i=1}^n W_i = n$ .

$\sigma_i$  is the standard deviation of the *i*th data point  $Y_i$  and *n* is the number of data points, or observations.

The principle behind nonlinear regression is to minimize the residual sum of squares by adjusting the parameters  $\hat{\beta}_j$  in the regression model to bring the curve close to the data points. This parameter is also referred to as the error sum of squares, or SSE. If the residual sum of squares is equal to 0.0, the curve passes through every data point.

Thus, the correlation that proposed to indicate the effect of those parameters on the polarization curve is:

$$V = a + bi^k + ciZ^n \left(\frac{T_{H_2}}{T_{cell}}\right)^d \left(\frac{T_{O_2}}{T_{cell}}\right)^e \left(\frac{\dot{Q}_{O_2}}{\dot{Q}_{H_2}}\right)^f P^g + lZ^h [\exp(m + pi)]^j \tag{3}$$

that in this equation current density is in A/cm<sup>2</sup>, temperatures are in °C, flow rates are in L/min, ambient pressure is in bar and *Z* = 2 for triangular channel.

In Eq. (3), the constants *a*, *b*, *c*, *d*, *e*, *f*, *g*, *h*, *j*, *k*, *l*, *m*, and *n* are undefined and using software as Datafit which fits the results of experiment from one to more independent variables that in Table 3, the value, upper limit and lower limit of constants in Eq. (3) was shown. Hence, by analyzing the results of experiments, Eq. (3) converts into

Eq. (4) as:

$$V = 0.8726 - 0.191i^{0.369} + 11.2024 \exp(-11.055 + 0.974i) - \frac{0.3152i}{P^{0.1327} \left(\frac{T_{H_2}}{T_{cell}}\right)^{0.0996} \left(\frac{T_{O_2}}{T_{cell}}\right)^{0.1375} \left(\frac{\dot{Q}_{O_2}}{\dot{Q}_{H_2}}\right)^{0.0269}} \tag{4}$$

Figure 9 shows the comparison between the experimental results and the correlated equation of the polarization curve for (a)  $T_{O_2} = 55^\circ\text{C}$ ,  $T_{H_2} = 55^\circ\text{C}$ ,  $T_{cell} = 60^\circ\text{C}$ ,  $P = 2.905$  bar,  $\dot{Q}_{O_2} = 0.5$  L/min,  $\dot{Q}_{H_2} = 0.3$  L/min and (b)  $T_{O_2} = 55^\circ\text{C}$ ,  $T_{H_2} = 55^\circ\text{C}$ ,  $T_{cell} = 60^\circ\text{C}$ ,  $P = 3.905$  bar,  $\dot{Q}_{O_2} = 0.5$  L/min and  $\dot{Q}_{H_2} = 0.3$  L/min. It is clear that there are significant agreements with them. Also, Fig. 10 shows the comparison between the experimental results of Miansari et al. [14] at *Z* = 3 and the 1 mm depth of the channels and the correlated equation at  $T_{O_2} = 70^\circ\text{C}$ ,  $T_{H_2} = 70^\circ\text{C}$ ,  $T_{cell} = 70^\circ\text{C}$  and  $P = 1.905$  bar. Also, it is clear that there are significant agreements with them.

Figure 11 shows the effect of inlet oxygen and hydrogen temperatures on the exergy efficiency of the PEM fuel cell at  $T_{cell} = 60^\circ\text{C}$ ,  $\dot{m}_{O_2} = 0.5$  L/min,  $\dot{m}_{H_2} = 0.3$  L/min and  $P = 2.905$  bar. Heat transfer, friction, mixing, chemical reactions, activation, ohmic and concentration polarizations can also increase thermodynamic irreversibility and decrease the exergy efficiency of PEM fuel cell. It can be seen that with the increase of oxygen and hydrogen temperatures, the exergy efficiencies of the cell increases. This is in fact due to the decrease in irreversible voltage losses of the cell with the increase of temperature, which in turn enhance the membrane conductivity and diffusion of proton in the membrane.

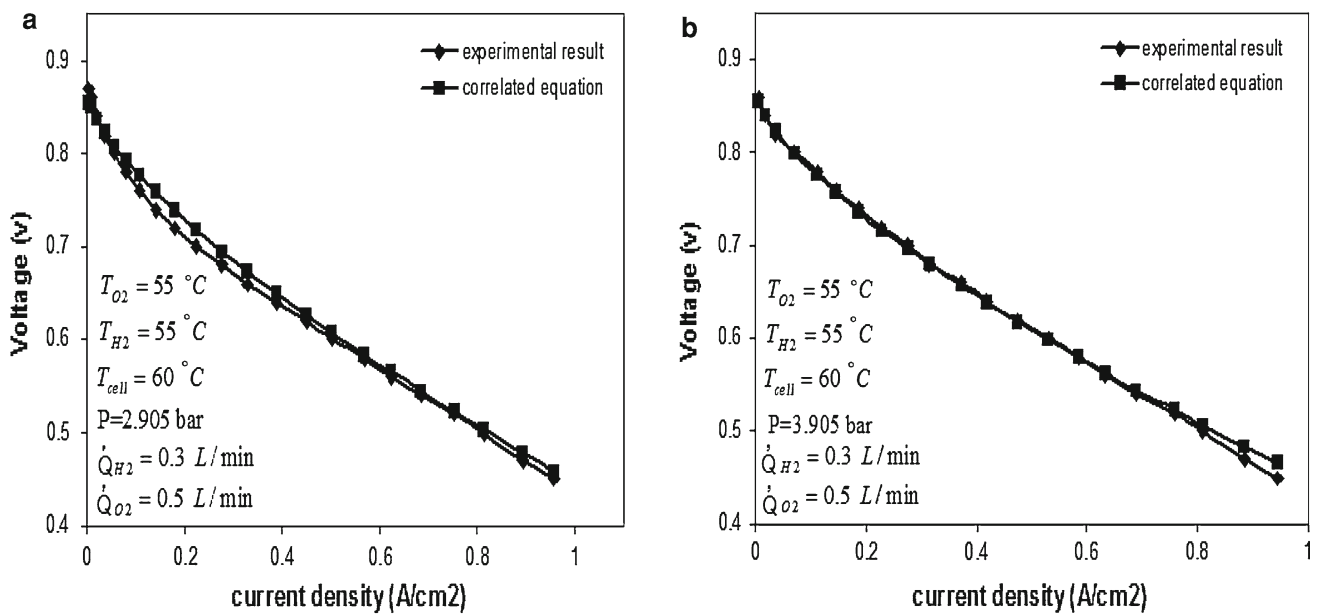


Fig. 9 Comparison between experimental results and results of correlated equation for a  $P = 2.905$  bar and b  $P = 3.905$  bar

Fig. 10 Comparison between experimental results of Miansari et al. [14] and results of correlated equation

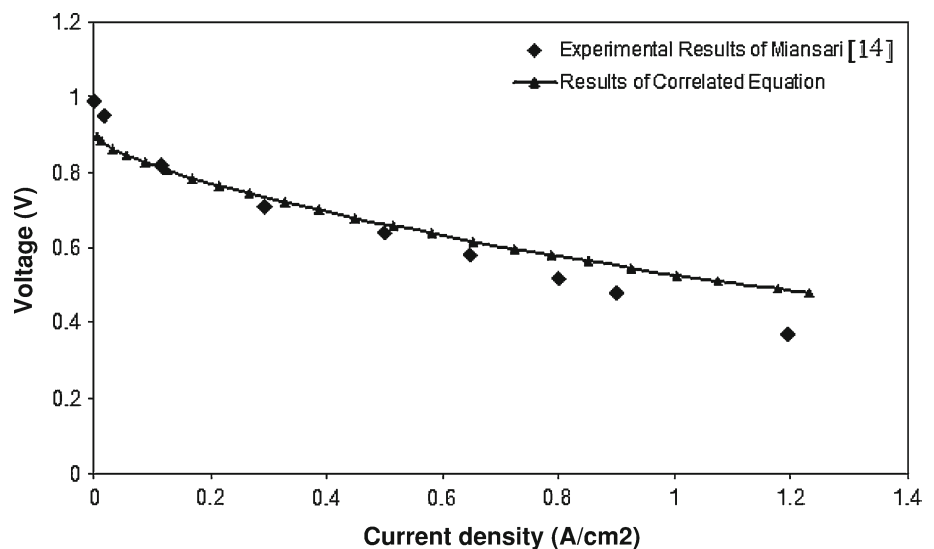


Figure 12 shows the effect of oxygen and hydrogen flow rates on the exergy efficiency of the PEM fuel cell at  $T_{cell} = 60\text{ }^\circ\text{C}$ ,  $T_{H_2} = 55\text{ }^\circ\text{C}$ ,  $T_{O_2} = 55\text{ }^\circ\text{C}$  and  $P = 2.905$  bar. It is clear that when the flow rate of oxygen is 0.9 L/min, the exergy efficiency is at higher value that this is due to increasing the output power of the cell at 0.9 L/min for oxygen flow rate. It is due to that by increasing the flow rate of oxygen, more oxidizer transport from GDL to the catalyst layer and the electrochemical reaction enhances. Also, it is clear that when the flow rate of hydrogen increases, the irreversibility of the cell increases but the exergy efficiency is at higher value at  $\dot{m}_{H_2} = 0.5$  L/min that this is due to increasing the output power of the cell at 0.5 L/min for hydrogen flow rate. It is due to that by increasing the flow rate of hydrogen, more

fuel transport from GDL to the catalyst layer and the electrochemical reaction enhances.

### 5 Conclusion

In this study, the effects of input oxygen ( $T_{O_2}$ ) and hydrogen temperatures ( $T_{H_2}$ ), cell temperature ( $T_{cell}$ ), input pressure ( $P$ ), oxygen ( $\dot{Q}_{O_2}$ ) and hydrogen flow rates ( $\dot{Q}_{H_2}$ ) on the performance and polarization curve of a triangular channel geometry PEM fuel cell have been investigated. We have found out that:

- With increasing the input gases pressure, the performance of the fuel cell increases which is due to decrease of ohmic

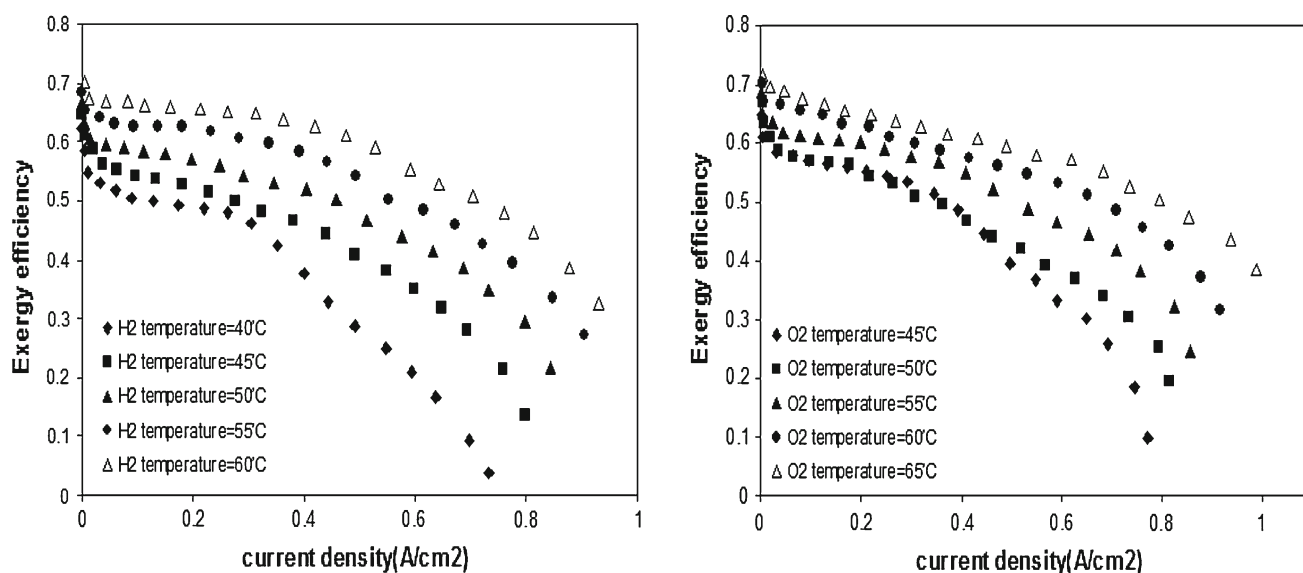


Fig. 11 Variation of exergy efficiency at different oxygen and hydrogen temperatures

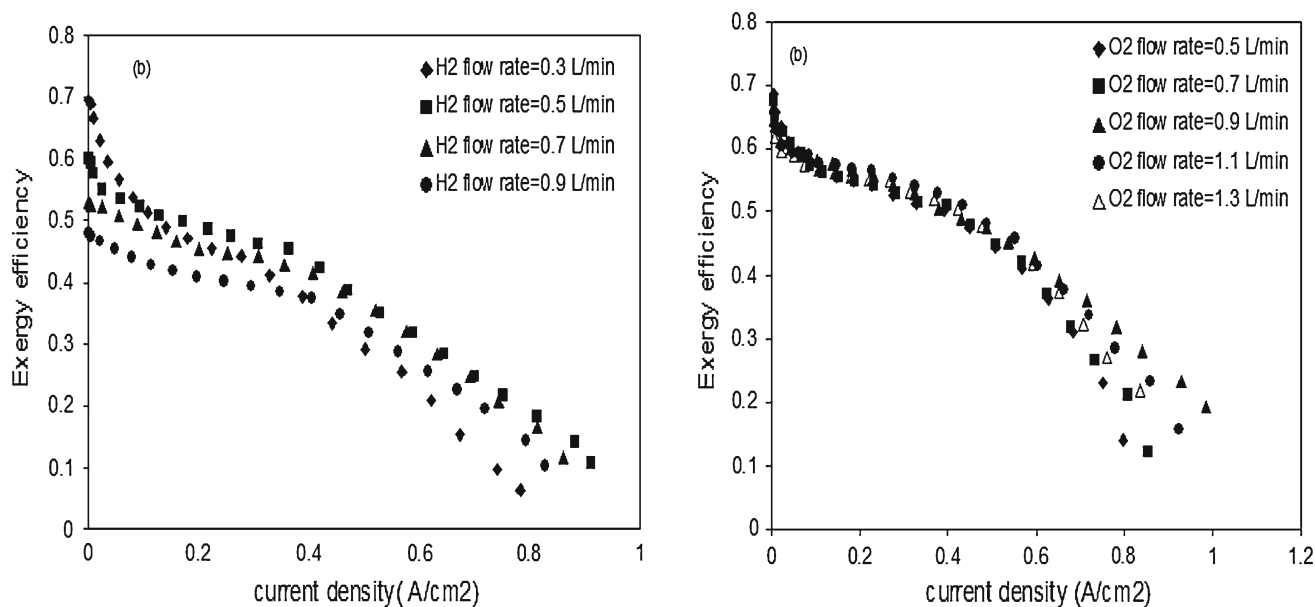


Fig. 12 Variation of exergy efficiency at different oxygen and hydrogen flow rates

and concentration losses and increase more efficient fuel transport from the GDL to catalyst layer.

- By increasing the hydrogen and oxygen flow rates, the cell performance enhances but when the flow rate increases from 0.7 to 0.9 L/min for hydrogen and from 0.9 to 1.3 L/min, the cell performance decreases.
- Increasing the cell temperature from 45 to 65 °C leads to the increase in the performance of the cell about 18 % which is due to the decreasing of activation overpotential and increase in the electrochemical reaction.

- The effect of oxygen and hydrogen temperatures on the performance of the cell is so important that by increasing the hydrogen and oxygen temperatures, the cell performance enhances about 20 % that it is due to the decreasing of activation overpotential and increase in the electrochemical reaction
- A new correlation for predicting the polarization curve of a PEM fuel cell according to input oxygen and hydrogen temperatures, cell temperature, input pressure, oxygen and hydrogen flow rates was proposed and there was a good

agreement between its results and the experimental results of Miansari et al. [14].

- When the flow rate of oxygen is 0.9 L/min, the exergy efficiency is at higher value which is due to increasing the output power of the cell at 0.9 L/min for oxygen flow rate.
- When the flow rate of hydrogen increases, the exergy efficiency is at higher value at  $\dot{m}_{H_2} = 0.5$  L/min.
- The effect of geometry of the fuel cell such as annular geometry and duct shaped geometry can be investigated experimentally.

**Acknowledgments** This work was partially supported by Renewable Energy Organization of Iran.

## References

1. Larminie, J.; Dicks, A.: Fuel cell system explained. 2nd edn., Wiley, New York (2003)
2. Scrivano, G.; Piacentino, A.; Cardona, F.: Experimental characterization of PEM fuel cells by micro-models for the prediction of on-site performance. *Renew. Energy*. **34**, 634–639 (2009)
3. Amphlett, J.C.; Baumert, R.M.; Mann, R.F.; Peppley, B.A.; Roberge, P.R.: Performance modeling of the Ballard Mark IV solid polymer electrolyte fuel cell. I—mechanistic model development. *Electrochem. Sci. Tech.* **142**, 1–8 (1995)
4. Mann, R.F.; Amphlett, J.C.; Hooper, M.A.I.; Jensen, H.M.; Peppley, B.A.; Roberge, P.R.: Development and application of a generalised steady-state electrochemical model for a PEM fuel cell. *J. Power Sources*. **86**, 173–180 (2000)
5. Del Real, A.J.; Arce, A.; Bordons, C.: Development and experimental validation of a PEM fuel cell dynamic model. *J. Power Sources*. **173**, 310–324 (2007)
6. Berning, T.; Djilali, N.: Three-dimensional computational analysis of transport phenomena in a PEM fuel cell—a parametric study. *J. Power Sources*. **124**, 440–452 (2005)
7. Yi, J.S.; Nguyen, T.V.: Multicomponent transfer in porous electrodes of proton exchange membrane fuel cells using the interdigitated gas distributors. *J. Electrochem. Soc.* **146**, 38–45 (1999)
8. Xue, D.; Dong, Z.: Optimal fuel cell system design considering functional performance and production costs. *J. Power Sources*. **76**(1), 69–80 (1998)
9. Ferng, Y.M.; Tzang, Y.C.; Pei, B.S.; Sun, C.C.; Su, A.: Analytical and experimental investigations of a proton exchange membrane fuel cell. *Int. J. Hydrogen Energy*. **29**, 381–91 (2004)
10. Hussain, M.M.; Baschuk, J.J.; Li, X.; Dincer, I.: Thermodynamic analysis of a PEM fuel cell power system. *Int. J. Thermal Sci.* **44**, 903–911 (2005)
11. Park, J.; Xianguo, L.: An experimental and numerical investigation on the cross flow through gas diffusion layer in a PEM fuel cell with a serpentine flow channel. *J. Power Source*. **163**, 853–863 (2007)
12. Jiao, K.; Park, J.; Xianguo, L.: Experimental investigations on liquid water removal from the gas diffusion layer by reactant flow in a PEM fuel cell. *Appl. Energy*. **87**, 2770–2777 (2010)
13. Park, J.; Xianguo, L.: Effect of flow and temperature distribution on the performance of a PEM fuel cell stack. *J. Power Source*. **162**, 444–459 (2006)
14. Miansari, M.; Sedighi, K.; Amidpour, M.; Alizadeh, E.; Miansari, M.O.: Experimental and thermodynamic approach on proton exchange membrane fuel cell performance. *J. Power Source*. **190**, 356–361 (2009)

